RAPID COMMUNICATIONS

PHYSICAL REVIEW B VOLUME 50, NUMBER 12 15 SEPTEMBER 1994-II

Giant magnetoresistance in lateral surface superlattices

G. Müller*
Max-Planck-Institut für Festkörperforschung, D-70569 Stuttgart, Germany

P. Středa
Institute of Physics, CZ-162 00 Praha, Czech Republic

D. Weiss and K. von Klitzing
Max-Planck-Institut für Festkörperforschung, D-70569 Stuttgart, Germany

G. Weimann
Walter-Schottky Institut der Technischen Universität München, D-85748 Garching, Germany

(Received 6 July 1994)

We investigate the low-field magnetoresistance ρ_{xx} perpendicular to a one-dimensional periodic potential which is imposed upon a two-dimensional electron gas in GaAs-$Al_xGa_{1-x}As$ heterojunctions. Distinct low-field anomalies and a crossover from positive to large negative magnetoresistance with increasing potential strength unveil the important role of anisotropic relaxation processes in strongly modulated electron systems.

Imposing a one-dimensional (1D) periodic potential upon a two-dimensional electron gas (2DEG) creates a lateral surface superlattice with peculiar transport properties.[1] The motion of conduction electrons in both a *weak* periodic potential (potential amplitude $V_0 \ll E_F$, the Fermi energy) and an applied magnetic field B perpendicular to the electron gas plane, for example, gives rise to magnetoresistance oscillations reflecting the interplay of the two relevant lengths of the system, the superlattice period a, and the classical cyclotron radius $R_c = \hbar k_F / eB$.[2] Here, $k_F = \sqrt{2\pi n_s}$ is the Fermi wave vector and n_s the carrier density of the 2DEG. These commensurability effects are usually accompanied by a pronounced *positive* low field magnetoresistance, if the current flows normal to the 1D modulation. The positive magnetoresistance stems from electrons on open orbits (parallel to the grating) and disappears once all electrons perform closed cyclotron orbits (magnetic breakdown). Usually the scattering time τ of the electrons is assumed to be the same in "valleys" and "hills" of the potential landscape. In this paper we demonstrate both experimentally and theoretically, that the slope of the magnetoresistance switches from positive to negative with increasing modulation strength. The understanding of this crossover involves not only the magnetic breakdown effect but also a $\vec{k}$-dependent scattering time, not considered previously.

We used conventional modulation doped GaAs-$Al_xGa_{1-x}As$ heterostructures containing a high mobility two-dimensional electron gas. A 1D lateral superlattice is defined by means of holographic lithography. The grating with period $a = 500$ nm is transferred to the 2DEG by selective wet etching of the GaAs cap layer. Hence the surface is either terminated by $Al_xGa_{1-x}As$ or by stripes of GaAs giving rise to an alternate bending of the conduction band which results in a lateral periodic potential.[3] After patterning we fabricated Hall bars, sketched in the inset of Fig. 1(b). To determine the resistivity ρ_{xx} we applied a dc current (0.1–0.5 μA) between the current probes [see Fig. 1(b), inset] and measured the longitudinal voltage drop using a nanovoltmeter. The magnetic field B was applied normal to the plane of the 2DEG. To change the modulation strength we used brief illumination with a red light emitting diode (LED) at liquid-helium temperatures.

Resistivity data, measured across the potential grating at 0.5 K, are displayed on the left-hand side of Figs. 1(a)–1(c) for different strengths of the modulation potential. For the strongest modulation [before LED flash, Fig. 1(a), left] the zero field resistivity is huge (74 kΩ), followed by a drastic *negative* low-field magnetoresistance if the magnetic field is ramped up. The symmetry of ρ_{xx} with respect to $\pm B$ reflects the homogeneity of our devices. Despite the large zero-field resistivity, quantum oscillations emerge at about $B = 1$ T. Reducing the modulation by briefly illuminating the sample with a LED, utilizing both, the persistent photoconductivity effect and the reduction of the surface depletion layer leads to a decrease of $\rho_{xx}(B=0)$ by a factor of ~ 7. This trace is plotted in Fig. 1(b) where the huge negative magnetoresistance from Fig. 1(a) now has changed to a more spiked helmetlike structure around $B = 0$. At higher B a pronounced resistance drop is still present just before the quantum oscillations commence. Further reduction of the modulation results in a camel's back shape of the resistivity, shown on the left-hand side of Fig. 1(c). Note that around $B = 0$ the resistance now *increases* (positive magnetoresistance) as is usually expected in lateral superlattices.

The right-hand side of Fig. 1 displays model calculations, discussed below. Our theoretical modeling is organized as follows: First, we sketch a model of the Fermi surface in a strong 1D periodic potential which has been presented in detail elsewhere.[7] Based on this picture we can (i) estimate the phase space fraction [determined by the angle θ in Fig. 2(c)] of electrons able to cross the potential grating, and (ii) derive the expressions Eqs. (6)–(9) for the conductivity. The central issue of our work is to demonstrate the consequences

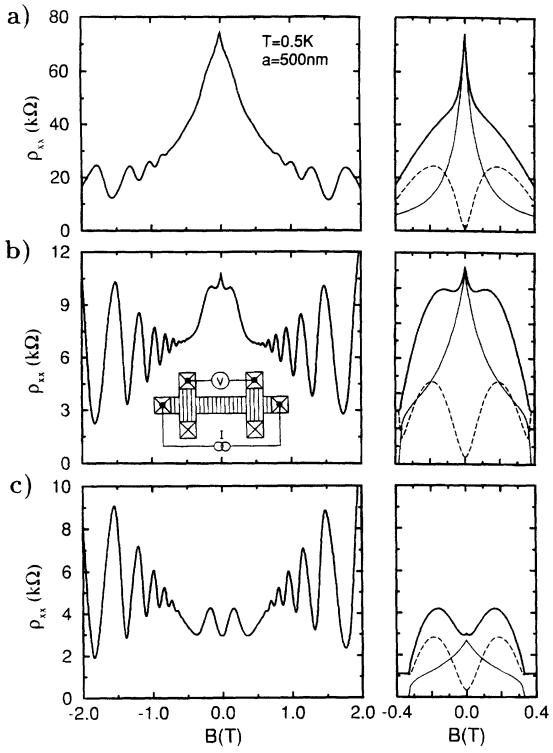

FIG. 1. Left-hand side: ρ_{xx} for different strengths of the one-dimensional superlattice potential. (a) Strongest, (b) intermediate, and (c) weakest modulation adjusted by brief illumination with a LED. The inset of (b) sketches the experiment. Right-hand side: Corresponding calculated ρ_{xx} traces (thick solid lines) consisting of isotropic (dashed) and anisotropic contributions (solid) to electron scattering rates. The parameters used are tabulated in Table I.

of different scattering times on the transport behavior. Based on simple assumptions we give explicit expressions for the magnetoresistance.

The unidirectional potential with period a in the x direction we model by a Kronig-Penney-type potential with amplitude $V_0/2$ and barrier width $a/2$, sketched in Fig. 2(a). Since the elastic mean free path (before patterning) is much larger than the period a, we expect the size quantization *within* the potential wells not to be destroyed by disorder. This is the origin of the peculiar Fermi surface which controls the transport properties. Generally, the electron energy $E(\vec{k})$ at $B=0$ may be written as

$$E(\vec{k})=\frac{\hbar^2 k_y^2}{2m^*}+\epsilon(k_x), \tag{1}$$

with k_x, k_y the wave-vector components and m^* the electron effective mass. The first term in Eq. (1) describes the free electron motion in the y direction. The second term in general is composed of 1D minibands due to Bragg reflections at the Brillouin zone boundaries. In the following we neglect Bragg reflection and consider only classical reflection. Since the period a is much larger than the Fermi wavelength $\lambda_F=2\pi/k_F\sim 0.1a$ semiclassical approximations may be used.

In the following we consider two distinct groups of electrons, *free* electrons and *bound* electrons. Only electrons with

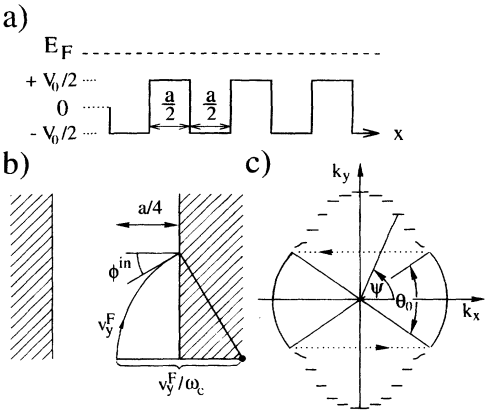

FIG. 2. (a) Sketch of our 1D model potential. (b) Angle of incidence ϕ^{in} used to estimate the B-dependent phase space fractions of *free* and *bound* electrons. (c) Calculated Fermi surface for $a=250$ nm, $V_0=7$ meV, and $E_F^{well}\equiv E_F+V_0/2=8.6$ meV. The dotted line describes the (classical) reflection of an electron from state $\pm k_x^F$ into $\mp k_x^F$ once the electron's angle of incidence (in real space) becomes too small to traverse the potential grating. Fermi wave vectors are different in the x and y direction: $k_y^F(\psi=\pi/2)$ corresponds to the density in the well region while $k_x^F(\psi=0)=k_F$ reflects the average carrier density. To see this consider an electron entering in (a) from the left with energy E_F: Then the Fermi surface derives from the $V_0=0$ case until the y-direction kinetic energy reaches $E_F-V_0/2$.

energies $\epsilon(k_x)$ higher than $+V_0/2$, have enough kinetic energy in the x direction to overcome the barrier. The corresponding segments of the Fermi surface, sketched in Fig. 2(c), remain circular with free-electron-like velocities: $v_x^F=\hbar k_F\cos(\psi)/m^*$ and $v_y^F=\hbar k_F\sin(\psi)/m^*$ for $-\theta_0/2\leq\psi\leq\theta_0/2$, and $\pi-\theta_0/2\leq\psi\leq\pi+\theta_0/2$. Here, k_F is the average Fermi wave vector corresponding to $V_0=0$ in Fig. 2(a), while the superscript F denotes the other quantities at the Fermi surface. The critical angle θ_0 dividing up the Fermi surface is determined by the condition $|k_x|=\sqrt{m^*V_0}/\hbar$, leading to $\cos(\theta_0/2)=\sqrt{V_0/2E_F}$. Significant deviations of $\epsilon(k_x)$ from the free electron dispersion $\hbar^2k_x^2/2m^*$ are expected if this energy is smaller than the barrier height. Electrons in these states are denoted as *bound* electrons, having a quantum-wire-like dispersion. The x component of the velocity expectation values for such classically bound electrons vanishes, giving rise to the flat sections at the Fermi surface with $v_x^F=0$ and $v_y^F=\hbar k_y^F(\psi)/m^*$ for $\theta_0/2\leq\psi\leq\pi-\theta_0/2$, and $\pi+\theta_0/2\leq\psi\leq 2\pi-\theta_0/2$, shown in Fig. 2(c). Since many Brillouin zones of our superlattice are occupied, we approximate $k_y^F(\psi)$ in the flat sections of the Fermi surface by

$$k_y^F(\psi)=\pm k_F\left(\frac{1+V_0/2E_F}{1+2\cot^2(\psi)}\right)^{1/2}. \tag{2}$$

Equation (2) interpolates between the limiting cases $k_y^F(\pi/2)=\sqrt{2m^*(E_F+V_0/2)}/\hbar$ and $k_y^F(\theta_0/2)=k_F\sin(\theta_0/2)$ in good agreement with exact numerical results of the Fermi surface.[4]

In magnetic fields the Lorentz force leads to a redistribution of the kinetic energy between the x and y directions. The

free electrons move along the states at the circular parts of the Fermi surface till they reach the boundary between *bound* and *free* states. Then a classical reflection occurs, $(k_x^F, k_y^F) \rightarrow (-k_x^F, k_y^F)$, forcing them to follow a closed trajectory in $\vec{k}$ space (and hence in real space), shown in Fig. 2(c). The *bound* electrons gain kinetic energy in the x direction which enables some of them to overcome the potential barrier and become *free*. This effect is known as the magnetic breakdown[5] which, for $2R_c \gg a/2$, can be treated classically.[6]

A *bound* electron becomes *free* when the sum of the acquired kinetic energy in the x direction, $m^*(v_x^{\rm in})^2/2$, and the miniband energy $\epsilon(k_x^F) = E_F - m^*(v_y^F)^2/2$ becomes larger than the barrier potential $V_0/2$. The equation

$$\epsilon(k_x^F) + \tfrac{1}{2} m^* (v_x^{\rm in})^2 = \frac{V_0}{2} \tag{3}$$

then defines a critical magnetic field to get over the barrier. To estimate $v_x^{\rm in}$ we consider an "average" electron in the middle of the well region which hits the barrier as is sketched in Fig. 2(b). The angle of incidence $\phi^{\rm in}$ and the velocity component $v_x^{\rm in}$ are

$$\sin\phi^{\rm in} = 1 - \frac{a\omega_c}{4 v_y^F}, \quad v_x^{\rm in} = v_y^F \cos\phi^{\rm in}, \tag{4}$$

where $\omega_c = eB/m^*$ is the cyclotron frequency. Using Eq. (4), and $v_y^F = \hbar k_y^F(\psi)/m^*$ we rewrite Eq. (3):

$$\frac{k_y^F(\psi)}{k_F} = \left(1 - \frac{V_0}{2E_F}\right)^{1/2} + \frac{m^*}{\hbar k_F}\frac{\omega_c a}{4}. \tag{5}$$

The $k_y^F(\psi)$ value, given by Eq. (2), which satisfies Eq. (5) determines the critical angle $\theta_B = 2\psi$ separating free and bound motion for *finite* magnetic field. In the following we model this magnetic breakdown effect[7] by replacing the angle θ_0 with θ_B. The angle θ_B increases as B grows indicating an increasing number of *free* and a decreasing number of *bound* electrons at the Fermi surface. For $\theta_B = \pi$, all electrons become *free*.

Assuming an *isotropic* relaxation time τ and weak magnetic fields ($\omega_c\tau \ll 1$), the Chamber's solution[8] of the Boltzmann equation may be used to evaluate the conductivity tensor. For the group of *free* electrons this involves the integration along the *closed* $\vec{k}$-space trajectory (circular parts) which gives

$$\sigma_{xx}^f = \frac{e^2 n_s \tau}{m^*}\frac{1 - C(\theta_B)}{1 + \omega_c^2\tau^2},$$

$$\sigma_{yy}^f = \frac{e^2 n_s \tau}{m^*}\frac{1 + \omega_c^2\tau^2 C(\theta_B)}{1 + \omega_c^2\tau^2} - \frac{e^2 n_s \tau}{m^*}\frac{\pi - \theta_B + \sin\theta_B}{\pi}, \tag{6}$$

where

$$C(\theta_B) = \frac{\pi - \theta_B}{\pi} - \frac{1 - \omega_c^2\tau^2}{1 + \omega_c^2\tau^2}\frac{\sin\theta_B}{\pi} + \frac{2}{\pi}\frac{\omega_c\tau}{1 + \omega_c^2\tau^2}(1 + \cos\theta_B)\frac{1 - \exp(-\theta_B/\omega_c\tau)}{1 + \exp(-\theta_B/\omega_c\tau)}. \tag{7}$$

The Hall conductivity is Drude-like, $\sigma_{xy}^f = -\sigma_{yx}^f = -\omega_c\tau\,\sigma_{xx}^f$. Here, the superscript f denotes quantities calculated for *free* electrons. The group of *bound* electrons (superscript b) contributes to the yy-conductivity component only, given by the sum over miniband contributions, $e^2 k_y^F(\psi)\tau/(\pi a m^*)$, and approximated by[7]

$$\sigma_{yy}^b = \frac{e^2 n_s \tau}{m^*}\frac{\pi - \theta_B + \sin\theta_B}{\pi}. \tag{8}$$

Inverting the total conductivity tensor, given as the sum of *free* and *bound* contributions, we obtain the resistivities for isotropic scattering (superscript iso):

$$\rho_{xx}^{\rm iso}(\tau) = \frac{m^*}{e^2 n_s \tau}\frac{1 + \omega_c^2\tau^2 C(\theta_B)}{1 - C(\theta_B)},$$

$$\rho_{yy}^{\rm iso}(\tau) = \frac{m^*}{e^2 n_s \tau}. \tag{9}$$

Here, the Hall resistivity equals the free electron value, $\rho_{xy}^{\rm iso} = B/e n_s$.

So far we assumed an isotropic scattering time. For strong modulation this assumption is not justified. Enhanced scattering is expected in low concentration regions where the screening of impurities is less effective.[9] These regions are accessible to *free* electrons only. We now ascribe different scattering times to free and bound electrons. Since bound ones cannot leave the well regions we describe scattering by the B-independent lifetime τ_0^b. The (B-dependent) lifetime τ^f of free electrons, exploring both well and barrier regions, we estimate by

$$\frac{1}{\tau^f} = \frac{\theta_0}{\theta_B}\frac{1}{\tau_0^f} + \frac{\theta_B - \theta_0}{\theta_B}\frac{1}{\tau_0^b}, \tag{10}$$

where τ_0^f denotes the zero-field value. Here, we assumed that the average (over phase space) scattering probability remains unchanged in weak magnetic fields.

Current conservation for a $\vec{k}$-dependent scattering time requires, in general, the numerical solution of the Boltzmann equation. Such numerics we avoid by introducing momentum relaxation times in the x and y direction, τ_x and τ_y. We neglect the magnetic field induced motion of states at the Fermi surface and describe the effect of the magnetic field by the angle θ_B. For $\omega_c\tau = 0$ we derive ρ_{xx} and ρ_{yy} by replacing τ in Eq. (6) and in Eq. (7) with τ^f, and in Eq. (8) with τ_0^b. Comparing the resulting ρ_{yy} with $\rho_{yy}^{\rm iso}$ [Eq. (9)] we obtain

$$\tau_y = \tau^f + \frac{\pi - \theta_B + \sin\theta_B}{\pi}(\tau_0^b - \tau^f). \tag{11}$$

Given the structure of $\rho_{yy}^{\rm iso}$, τ_y can be viewed as the "isotropic" scattering time of our inhomogeneous system. Hence we express the resistivity in the x direction as

$$\rho_{xx} = \rho_{xx}^{\rm iso}(\tau_y) + \Delta\rho_{xx}, \tag{12}$$

TABLE I. Parameters of the model calculations shown in Fig. 1.

	n_s^{well} (cm^{-2})	E_F^{well} (meV)	V_0 (meV)	τ_0^f (ps)	τ_0^b (ps)
Fig. 1(a)	2.36×10^{11}	8.1	7.8	0.081	7.5
Fig. 1(b)	2.51×10^{11}	8.6	7.0	0.22	7.5
Fig. 1(c)	2.63×10^{11}	9.0	6.7	0.67	7.5

where, for $(\omega_c\tau=0)$ we find

$$\Delta\rho_{xx}=\frac{m^*}{e^2 n_s \tau_y}\,\frac{\pi-\theta_B+\sin\theta_B}{\theta_B+\sin\theta_B}\,\frac{\tau_0^b-\tau^f}{\tau^f}\,. \tag{13}$$

While $\rho_{xx}^{\text{iso}}(\tau_y)$ in Eq. (12) is valid for finite $\omega_c\tau$, Eq. (13) strictly holds only for $\omega_c\tau=0$. If, however, we assume the enhanced scattering in the barrier region to take place within infinitesimally narrow stripes, Eq. (13) also holds for $\omega_c\tau\neq0$. Due to the huge aspect ratio only the transport coefficients in the x but not in the y direction are altered. Such an approach idealizes our system but allows us to derive analytic expressions for the magnetoresistance; however, it neglects the influence of anisotropic scattering on the Hall resistivity.

The results of the model calculations are shown on the right-hand side of Fig. 1 where we plot both the isotropic contribution ρ_{xx}^{iso} and the correction term $\Delta\rho_{xx}$. The resulting total resistivity, $\rho_{xx}^{\text{iso}}+\Delta\rho_{xx}$, closely follows the experimental traces. The magnetoresistivity ρ_{xx}^{iso}, *always* positive and followed by a breakdown peak, dominates for the weakest modulation in Fig. 1(c) as is manifested in the camel's back shaped low B magnetoresistance trace. With increasing modulation strength the anisotropic scattering effect, accounted for by $\Delta\rho_{xx}$, dominates. This is the origin of the pronounced negative magnetoresistance in Fig. 1(a) and the "spiked helmet" in Fig. 1(b).[10]

The parameters used in our calculations are summarized in Table I. The quantum oscillations observed in the experiments we ascribe to Shubnikov–de Haas (SdH) oscillations within the potential wells. Hence, the Fermi energy inside the well, $E_F^{\text{well}}\equiv E_F+V_0/2$, can be extracted from the periodicity of the SdH oscillations. The scattering time of bound electrons, τ_0^b, is controlled by "boundary" scattering and is hence assumed to be the same for all three modulation strengths. The barrier height V_0 and the scattering time τ_0^f of free electrons remain as fit parameters. The fit parameters we obtain are reasonable: τ_0^b, the scattering time *in* the well, is comparable to the one measured in the unpatterned 2DEG. Also the fitted values of τ_0^f behave as expected[9] and drastically decrease with increasing potential amplitude V_0.

Despite the simplifications, our model covers essentially all the low B features observed in experiment.[11] The abrupt decrease of the calculated magnetoresistance traces at $\theta_B=\pi$ is the result of the strict distinction between the two groups of electrons. A more advanced model, employing finite probabilities for electrons to be *free* or *bound*, could result in a more gradual resistance drop, shown previously for weak periodic potentials.[12]

In summary we have shown that the low B resistance anomalies in lateral superlattices with strong potential modulation arise from the anisotropy in $\vec{k}$ space. Aside from the different electron dynamics on "free" and "bound" Fermi surface segments, the explanation of the negative magnetoresistance necessitates the introduction of $\vec{k}$-dependent relaxation rates, i.e., different scattering times for *free* and *bound* electrons. With increasing B the anisotropy of the Fermi surface and hence the low field anomalies vanish.

We thank R. Fleischmann, R. R. Gerhardts, and F. Stern for valuable discussions. Work was supported by BMFT Grant No. 01BM121/8. P.S. acknowledges support by the NATO collaborative research Grant No. CRG921204.

*Present address: AT&T Bell Laboratories, 600 Mountain Ave, Murray Hill, NJ 07974.

[1] For reviews see C. W. Beenakker and H. van Houten, in *Solid State Physics*, edited by H. Ehrenreich and D. Turnbull (Academic, Boston, 1991), Vol. 44; D. K. Ferry, Prog. Quantum Electron. **16**, 251 (1992); W. Hansen, J. P. Kotthaus, and U. Merkt, in *Semiconductors and Semimetals*, edited by R. K. Willardson, A. C. Beer, and E. P. Weber (Academic, San Diego, 1992), Vol. 35.

[2] D. Weiss, K. v. Klitzing, K. Ploog, and G. Weimann, Europhys. Lett. **8**, 179 (1991).

[3] K. Lier and R. R. Gerhardts, Phys. Rev. B **48**, 14 416 (1993).

[4] P. Středa, J. Kučera, and J. van de Konijnenberg, Phys. Scr. **T39**, 162 (1991).

[5] P. Středa (unpublished).

[6] R. W. Stark and L. M. Falicov, Prog. Low-Temp. Phys. **5**, 235 (1967).

[7] P. H. Beton, E. S. Alves, P. C. Main, L. Eaves, M. W. Dellow, O. H. Hughes, S. P. Beaumont, and C. D. W. Wilkinson, Phys. Rev. B **42**, 9229 (1990).

[8] R. G. Chambers, Proc. Phys. Soc. London Sect. A **81**, 877 (1963). See also N. W. Ashcroft and N. D. Mermin, *Solid State Physics* (Saunders College, Philadelphia, 1976).

[9] For homogeneous 2DEG's typically $\tau\sim n_s^\gamma$ with $\gamma\sim1.1-1.7$ holds. See, K. Hirakawa and H. Sakaki, Phys. Rev. B **33**, 8291 (1986).

[10] Negative magnetoresistance caused by weak localization is discussed by J. R. Gao, C. de Graaf, A. S. Schüssler, J. Caro, S. Radelaar, and K. Heyers, Phys. Rev. B **46**, 9885 (1992).

[11] Deviations with respect to the B scale in Fig. 1(a) can be attributed to depletion regions around the etched stripes making the well smaller than $a/2$. This shifts the ρ_{xx} features, as in experiment, towards higher B.

[12] P. Středa and A. H. MacDonald, Phys. Rev. B **41**, 11 892 (1990).